Dynamics of a single particle in a horizontally shaken box

Barbara Drossel and Thomas Prellberg *
Department of Theoretical Physics, University of Manchester, Manchester M13 9PL, UK
(November 13, 2000)

We study the dynamics of a particle in a horizontally and periodically shaken box as a function of the box parameters and the coefficient of restitution. For certain parameter values, the particle becomes regularly chattered at one of the walls, thereby loosing all its kinetic energy relative to that wall. The number of container oscillations between two chattering events depends in a fractal manner on the parameters of the system. In contrast to a vertically vibrated particle, for which chattering is claimed to be the generic fate, the horizontally shaken particle can become trapped on a periodic orbit and follow the period–doubling route to chaos when the coefficient of restitution is changed. We also discuss the case of a completely elastic particle, and the influence of friction between the particle and the bottom of the container.

1. INTRODUCTION AND SUMMARY

While vertically shaken granular materials have been the object of intensive research in the past years, the investigation of horizontally shaken granular materials has just started [1,2]. Vertically shaken materials show various cellular patterns and localized oscillons [3–5], and their horizontal counterpart was recently found to display ripple–like patterns [1]. Since these patterns are due to the collective behaviour of many interacting particles, the one–particle system shows completely different phenomena that are, however, equally fascinating. The dynamical evolution of a bouncing ball on a vibrating platform was studied in [6,7]. As long as the coefficient of restitution is smaller than one, a particle that hits the platform with sufficiently small relative velocity bounces off the platform infinitely often during a finite time and looses its memory of earlier dynamics. The authors of [7] argue that this "chattering" is the fate of generic trajectories, which therefore become periodic. They conclude that true chaos cannot be observed in this system.

In this paper, we study the dynamics of a singe particle in a horizontally shaken box. While chattering occurs for part of the parameter values and initial conditions, we find as well other generic scenarios like periodic orbits without chatter, the period–doubling route to chaos, and strange attractors. The interplay between these different modes of behaviour makes this apparently simple system astonishingly rich and fascinating.

The outline of this paper is as follows: In the next section we define the system used in our simulations. In section 3 we discuss the limiting case of a completely inelastic particle that assumes the velocity of the wall at each collision. When the particle hits the wall during the half period where the wall accelerates toward it, it sticks to the wall until the end of the half period. The number of reflections until this locking occurs depends in a fractal manner on the parameter of the system. We also discuss the influence of friction between the particle and the bottom of the container. Next, the opposite limit of a completely elastic particle is considered in section 4. This system displays all signatures of Hamiltonian chaotic systems, including periodic, quasiperiodic, and chaotic orbits. The physically most relevant case of a partially elastic particle is then studied in section 5. On the one hand, increasing the coefficient of restitution from zero, the period–doubling route to chaos is observed in many cases. Ultimately, the strange attractor becomes so large that it includes the chattering region, thus making the orbits again periodic. On the other hand, decreasing the coefficient of restitution from one, the neutrally stable fixed points become attractive. All irrational tori disappear and all trajectories appear to first become periodic. A trajectory starting in the locking region may or may not lead back to it, and several periodic orbits coexist, their basins of attraction being strongly interwoven. Section 6 concludes the paper.

2. THE MODEL

The left and right wall of a horizontally shaken container of length L are described by the equations

$$x_{\text{leftwall}} = A\sin(\omega t)$$
$$x_{\text{rightwall}} = L + A\sin(\omega t)\,.$$

ω is the frequency, and A the amplitude of shaking. We denote position and velocity of the particle by x and v respectively, and introduce the relative position and velocity with respect to the container walls

*email: drossel@a13.ph.man.ac.uk, prel@a13.ph.man.ac.uk

$$l = x - A\sin(\omega t) \quad , \quad u = v - A\omega\cos(\omega t)\ . \tag{1}$$

Between collisions, the particle moves according to a linear friction law $dv/dt = -\gamma u$, i.e.,

$$du/dt = -\gamma u + A\omega^2 \sin(\omega t)\,, \tag{2}$$

with a friction coefficient γ which will be set equal to zero in most parts of this paper.

The collisions with the wall are partially inelastic, and the relative velocity u changes according to

$$u' = -\eta u \tag{3}$$

at each collision, where η is the coefficient of restitution.

It is convenient to measure the particle position in units of the amplitude A, time in units of the inverse frequency ω^{-1}, and velocity in units of $A\omega$. Then the system can be described by the dimensionless parameters $\alpha = L/A$, $\tilde{\gamma} = \gamma/\omega$, and η. We denote the dimensionless time, length, and velocity again by t, l, and u. We also introduce the phase of the container oscillation $\phi = \omega t \bmod 2\pi$.

The motion of the particle can be written down immediately. It is most convenient to describe the particle dynamics in terms of a map that gives the phase of the container oscillation and the particle velocity immediately after an impact as function of their values immediately after the previous impact. Let the particle leave the left wall ($l = 0$) after an impact at $t = t_0$ with a relative velocity u_0. The particle moves according to

$$\begin{aligned} l_{t_0,u_0}(t) &= \frac{1}{\tilde{\gamma}}(\cos t_0 + u_0) - \frac{1}{\tilde{\gamma}^2+1}(\sin t + \tilde{\gamma}\cos t) \\ &\quad - \left(u_0 - \frac{1}{\tilde{\gamma}^2+1}(\tilde{\gamma}\sin t_0 - \cos t_0)\right) \\ &\quad \times \frac{1}{\tilde{\gamma}}\exp(-\tilde{\gamma}(t-t_0))\,, \end{aligned} \tag{4}$$

the corresponding velocity being $u = dl/dt$. We will mainly discuss $\gamma = 0$, where this equation reduces to

$$l_{t_0,u_0}(t) = \sin t_0 - \sin t + (u_0 + \cos t_0)(t - t_0)\ . \tag{5}$$

The next collision occurs at the smallest solution $t_c > t_0$ of

$$l_{t_0,u_0}(t_c) \;=\; 0 \qquad \text{impact at same wall} \tag{6a}$$
$$l_{t_0,u_0}(t_c) \;=\; \alpha \qquad \text{impact at other wall} \tag{6b}$$

at which the velocity is $u_c = u_{t_0,u_0}(t_c)$. If the particle impacts again the same wall, the new velocity is now $u_1 = -\eta u_c$. On the other hand, if the particle collides with the right wall, it is convenient to use the symmetry between left and right wall to map the right wall to the left wall via $t \to t - \pi$ and $l \to \alpha - l$, so that now $u_1 = \eta u_c$. The velocity is thus always measured with respect to the wall at which the last impact has occurred.

Given an initial phase $\phi_0 = t_0$ and velocity u_0, we thus arrive at the map

$$\phi_1 \;=\; t_c \bmod 2\pi\,, \quad u_1 = -\eta u_c \qquad \text{impact at same wall} \tag{7a}$$
$$\phi_1 \;=\; (t_c - \pi) \bmod 2\pi\,, \quad u_1 = \eta u_c \qquad \text{impact at other wall} \tag{7b}$$

Before we will study this mapping in detail below, we shall briefly discuss the case of no dissipation ($\eta = 1$ and $\gamma = 0$). Here, the dynamics can be derived from a time–dependent Hamiltonian [8,9]

$$H = \frac{p^2}{2m} + V_{SQ}(q) + Am\omega^2 q \sin(\omega t)\,, \tag{8}$$

where $V_{SQ}(q)$ is a square–well potential describing the walls at $q = 0$ and L, and m and p are mass and momentum of the particle. The last term in the Hamiltonian (8) causes a periodic oscillation of the particle with respect to the walls. (Since we describe the system in terms of relative coordinates and velocities between the particle and the wall, a system with periodically oscillating walls and a system with a periodic particle oscillation superimposed to the ballistic motion are equivalent.) Measuring p in units of $mL\omega$, H and V in units of $mL^2\omega^2$, q in units of L, and t in units of ω^{-1}, , we arrive at a dimensionless formulation,

$$H = \frac{p^2}{2} + v_{SQ}(q) + \frac{q}{\alpha}\sin t \tag{9}$$

where $v_{SQ}(q)$ is an appropriately scaled square well potential with walls at 0 and 1. Upon introducing action–angle variables (J, θ) for the "unperturbed" Hamiltonian $H_0 = p^2/2 + v_{SQ}(q)$ [8,9], the Hamiltonian (9) transforms to

$$H = \frac{\pi^2 J^2}{2} + \alpha^{-1}\left(\frac{1}{2}\sin t + \frac{2}{\pi^2}\sum_{\substack{n=-\infty \\ n\ odd}}^{\infty} \frac{1}{n^2}\sin(n\theta - t)\right) \tag{10}$$

The transformation between (p, q) and (J, θ) is given by

$$p = \pi J \,\mathrm{sign}\,\theta \quad \text{and} \quad q = |\theta|/\pi \tag{11}$$

for $-\pi < \theta < \pi$, and periodically continued in θ. We have included the term $(2\alpha)^{-1}\sin t$ in the Hamiltonian (10) for completeness sake, but we shall drop it below as it does not influence the dynamics.

3. THE COMPLETELY INELASTIC PARTICLE

3.1. Modelling by a one–dimensional map

We now discuss the case $\gamma = 0$ and $\eta = 0$ in detail. The particle moves freely between the walls, and after an impact the relative velocity u_0 with respect to the wall is zero. This means that the two–dimensional mapping defined above is in fact reduced to a one-dimensional mapping. The subsequent fate of the particle depends only on the phase ϕ_0 at the moment of impact, as indicated in Fig. 1.

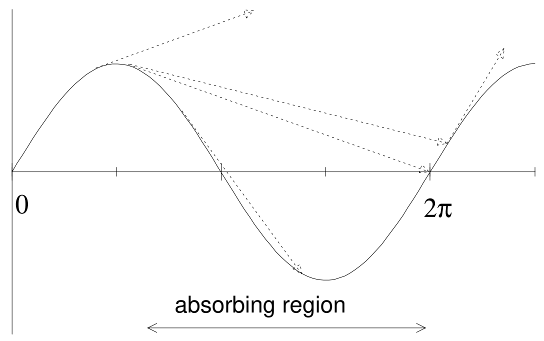

FIG. 1. The fate of a particle that is inelastically reflected at the wall.

For $\phi_0 \in [0, \pi/2[\bmod 2\pi$, the particle is reflected from the wall with (absolute) velocity $\cos(\phi_0)$ and is headed for the other wall. For $\phi_0 \in [\pi, 2\pi[\bmod 2\pi$, the particle sticks to the wall until $\phi_0 = 2\pi$, and then leaves the wall with (absolute) velocity 1. In the intermediate region $\phi_0 \in]\pi/2, \pi[\bmod 2\pi$, the sign of the particle velocity is not reversed during the collision, and the particle hits the same wall again at a later phase ϕ_1 which is determined by the equations (5), (6a), and (7a), leading to

$$\sin\phi_0 - \sin\phi_1 + (\phi_1 - \phi_0)\cos\phi_0 = 0\,. \tag{12}$$

For $\phi_0 \geq \phi^c = 1.79..$, the phase ϕ_1 is in the locking interval $[\pi, 2\pi[$. As we are interested in the dynamics between impacts at opposite walls, we can extend the locking interval to include ϕ^c, i.e., to the interval $[\phi_c, 2\pi]$. For $\phi_0 < \phi^c$, the phase ϕ_1 is in the interval $[0, \pi/2[\bmod 2\pi$ and the particle is immediately reflected towards the other wall, where it arrives at a phase ϕ_2 now given by (6b) and (7b), i.e.,

$$\sin\phi_1 + \sin\phi_2 + (\phi_2 - \pi - \phi_1)\cos\phi_1 = \alpha\,. \tag{13}$$

From now on, let ϕ_i denote the phase of a wall at the moment where the particle is reflected towards the other wall for the ith time. We do not count reflections that lead to a subsequent reflection at the same wall. Then, the map that gives ϕ_{i+1} as function of ϕ_i is a map of the interval $[0, \pi/2[$ into itself, dependent only on the dimensionless parameter $\alpha = L/A$. The map $\phi_{i+1} = \Phi_\alpha(\phi_i)$ is given implicitly by the equations (12) and (13), and is shown in Fig. 2 for the value $\alpha = 5$. Branches with positive slope correspond to a particle arriving at the other wall at a phase in the interval $[0, \pi/2]$, from where it is immediately reflected back, while branches with negative slope indicate a twofold reflection at the other wall, the first reflection being in the phase interval $]\pi/2, \phi^c]$. The dashed line is the diagonal $\phi_{i+1} = \phi_i$, and the dotted line indicates the fate of a particle starting at phase zero. For $\pi/2 > \phi_i > \pi - \phi^c$, the velocity of the particle is so small that it cannot hit the other wall in the locking region. A small interval $\Delta\phi_i$ maps onto an interval $\Delta\phi_{i+1}$ proportional to the flight time, which is of the order $\alpha/\cos\phi_i$. For this reason, the density of branches in the map increases with increasing α and ϕ_i and diverges when ϕ_i approaches the value $\pi/2$, where the initial velocity decreases to zero.

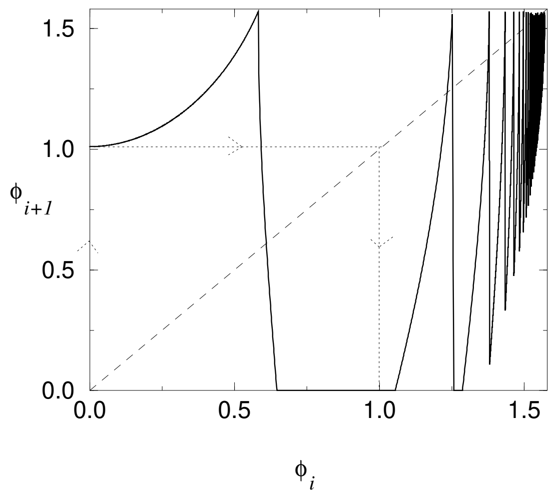

FIG. 2. The map for $\alpha = 5$.

3.2. Periodic trajectories

The phase $\Phi_\alpha(0)$ at which a particle starting at phase zero will be reflected from the other wall depends on α. It is zero for $\alpha \in [(2n-1)\pi + \phi^c + \sin\phi^c, (2n+1)\pi]$, for any nonnegative integer n. In this case, a particle that starts in the locking region will hit the locking region at the other wall, and the periodicity of such a trajectory is one. For all values of α, the map intersects the perpendicular axis with a slope zero, since the initial velocity does not change with ϕ_i for $\phi_i = 0$. For values α only slightly above $(2n+1)\pi$, the map therefore has a stable fixed point $\phi^\star$ close to zero. This fixed point vanishes with increasing α via a saddle–node bifurcation, and for values of α slightly beyond the bifurcation, a particle trajectory can be trapped for a long time in the neighborhood of the former fixed point, before it escapes and hits ultimately the locking region where $\phi_{i+1} = 0$. Due to these locking regions, there exist no truly chaotic trajectories, but each trajectory has a finite periodicity. When α increases further, the number of reflections in the neighborhood of the former fixed point (or, more precisely, on the first branch that has positive slope), decreases in steps of size one. Close to such a decrease, a trajectory that leaves the first branch goes through the upper right–hand corner of the map and can therefore have an arbitrarily large periodicity. Further away from it, a trajectory can hit the locking region immediately after leaving the first branch. In general, very complex trajectories can occur. In particular when $\Phi_\alpha(0)$ is close to $\pi/2$, the trajectory will spend some time in the upper right–hand corner of the map, and a slight change in α may lead to a large change in the periodicity of the trajectory.

There are also many possibilities for obtaining low–periodicity trajectories. In Fig. 2, e.g., the periodicity is two. A period–doubling bifurcation sequence occurs when α is decreased from $(2n-1)\pi + \phi^c + \sin\phi^c$. In Fig. 3, this scenario is sketched. Since it involves only the first two branches of the map, the other branches are not shown. As long as the first branch is small (e.g., for $\alpha = 5.8$), the particle hits the locking region after the second reflection. With decreasing α, the endpoint of the trajectory moves to the right, and finally hits the foot of the second branch, leading to a period–doubling bifurcation. For $\alpha = 5.743$, one observes therefore a cycle of period 4. When α is decreased further, the end point of the 4–cycle moves to the left and hits the foot of the first branch, leading to another period doubling.

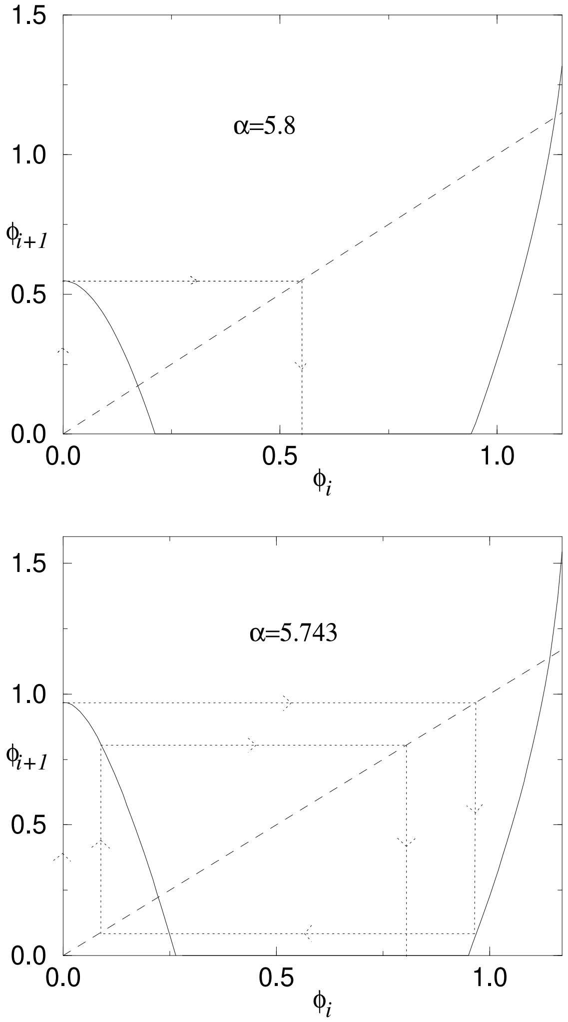

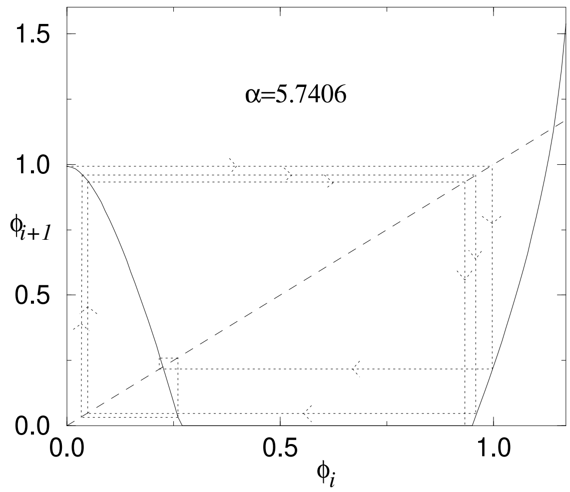

FIG. 3. A series of bifurcations when α is decreased.

The last part of Fig. 3 shows an 8–cycle for $\alpha = 5.7406$. This period–doubling scenario continues as the end point of the 8–cycle moves to the left, etc., and the period becomes infinite when the trajectory hits the unstable fixed point on the first branch. For even smaller values of α, other periodicities are observed that are not powers of 2.

Fig. 4 shows the period of a trajectory originally starting in the absorbing region as function of α.

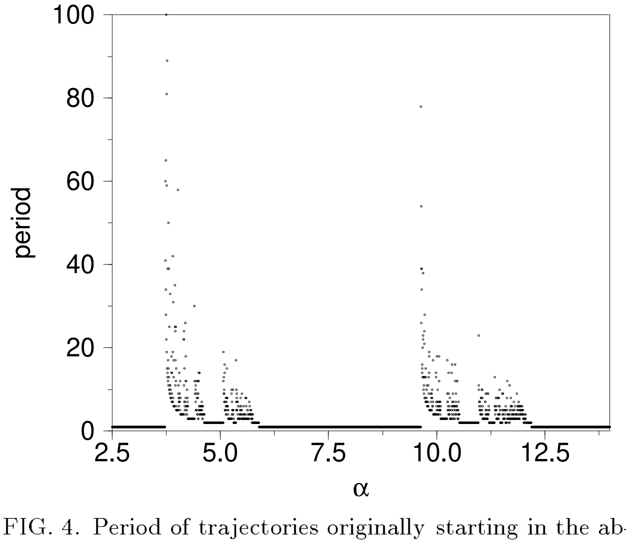

FIG. 4. Period of trajectories originally starting in the absorbing region as function of α.

All the above–mentioned features can be seen: The large plateaus of period 1 that extend beyond $(2n+1)\times\pi$ because of the existence of stable periodic orbits outside the locking region; the stepwise decrease of the number of subsequent reflections at the first branch as α increases, and a high periodicity in between these subsequent plateaus; the trajectory of period 2 shown in Fig. 2; the period–doubling sequence at the left end of the period–1 plateaus (due to the finite resolution in α only the 2– and 4–cycles can be seen. The 3–cycle lies beyond the period–doubling sequence). As the branches of the map become steeper and more numerous with increasing α, plateaus will become shorter, and the structures will become more complex for large α.

3.3. Comparison to a vertically shaken particle

In [6,7], the periodicity of trajectories of vertically shaken completely inelastic particles is studied. There, gravitation brings the particle back to the vibrating platform, and no second wall is needed. Therefore, fast particles have longer flight times between reflections than slow particles, while the opposite holds for horizontally shaken particles. For large oscillation frequencies, the authors of [6] obtain an approximate map of the form $\phi_{i+1} \simeq \phi_i + const. \times \cos\phi_i$. An approximate map for our system is obtained from Eq. (13) for large α and reads $\phi_{i+1} \simeq \phi_i + \pi + \alpha/\cos\phi_i$. The map in [6] has no stable fixed points and no region where the trajectory can be temporarily trapped. Nevertheless, there are infinite hierarchies of periodic trajectories between low–period plateaus, leading to a structure on all scales of the period–vs–frequency plot, as for the horizontally shaken particle.

3.4. The influence of friction

In the presence of friction between the particle and the container bottom, there exist stable low–velocity particle trajectories that never touch the walls, but move periodically back and forth in a small region somewhere in the central part of the container. Particles that are reflected at a phase near $\pi/2$ have a very small velocity and can become trapped in such a region. Apart from the locking sections in the map Fig. 2, there is consequently an absorbing section for ϕ_i above some threshold that depends on α and the strength of friction. From equation (4) with $u_0 = 0$ we see that the maximum possible value of l is

$$l^{\max}_{\phi_0,0} = \frac{1}{\tilde{\gamma}} \cos\phi_0 + \frac{1}{\sqrt{1+\tilde{\gamma}^2}} \ . \quad (14)$$

The first term is the initial velocity divided by the friction coefficient, and is the distance that a particle with initial velocity $\cos(\phi_0)$ can travel on a stationary surface. The second term is the amplitude of the periodic oscillation that a particle performs when it is periodically driven. If $l^{\max}_{\phi_0,0} < \alpha$, the particle never reaches the other wall. If $\alpha > 1$, this is always the case for ϕ_0 close enough to $\pi/2$, as the initial (absolute) velocity of the particle is arbitrarily small. If α is large enough, i.e.,

$$\alpha > \frac{1}{\tilde{\gamma}} + \frac{1}{\sqrt{1+\tilde{\gamma}^2}} \ , \quad (15)$$

then even a particle that was reflected at phase zero, i.e., with maximum velocity, does not reach the other wall. Fig. 5 shows the period of trajectories as function of α for $\tilde{\gamma} = 0.025$.

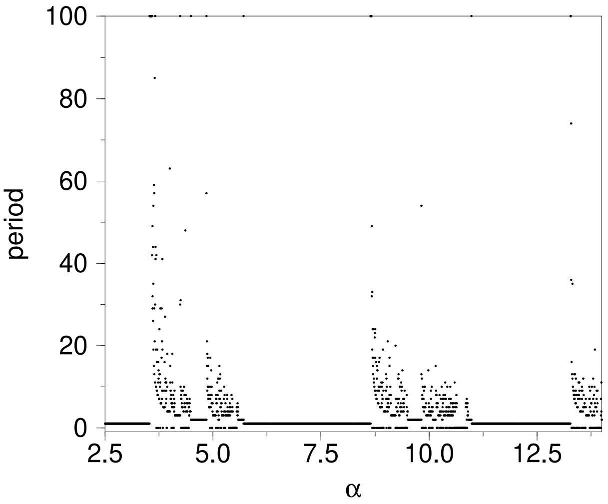

FIG. 5. Period of trajectories originally starting in the absorbing region as function of α, with a friction coefficient $\tilde{\gamma} = 0.025$.

Trajectories that get stuck in the absorbing region are assigned a period zero. To keep the computer program simple, friction was only active for x–coordinates between 1 and $\alpha - 1$, and only leading terms in $\tilde{\gamma}$ were considered. Comparing Fig. 5 with Fig. 4, one finds that with increasing α the graph becomes more and more compressed horizontally, and that an increasing fraction of trajectories get stuck. The region $\alpha > 41.0$ where all trajectories get stuck, is not shown on the graph.

4. THE COMPLETELY ELASTIC PARTICLE

We now study the non-dissipative case $\eta = 1$ and $\gamma = 0$. Here, the particle moves without friction and is reflected elastically at the container walls, where its relative velocity with respect to the wall changes sign at each collision. The velocity is now an independent variable, adding a new dimension to the phase space. As the system is non-dissipative, it can be described by a time–dependent Hamiltonian as described in section 2. An equivalent problem is studied in [8–10], namely the motion of a charged particle in a one–dimensional infinite square well potential driven by an oscillating external field. In those papers, the particle performs periodic oscillations (superimposed to the free motion). The parameter α^{-1} is proportional to the electric field. In terms of coordinates and velocities relative to the container walls, the dynamics is the same as for our system.

Since the system is hamiltonian, phase space volume is conserved in time, and a stroboscopic Poincare section that gives $l(t)$ and $u(t)$ in time intervals $T = 2\pi$ is area preserving. However, we find it physically more relevant to plot the phase of the oscillation and the velocity of the particle relative to the wall immediately after each reflection, i.e. $\phi = t_c \bmod 2\pi$ and $u(t_c)$ for $l(t_c) = 0$. As the time intervals are not constant, this representation is not area preserving, but describes of course the same physics as a true Poincare section. Fig. 6 shows our data points for $\alpha = 1.65$, $\alpha = 16.5$, and $\alpha = 165$, and for several different trajectories. The value of α used in [8–10] is of the order of several hundred, since the authors were mainly interested in the limit of small electrical field.

In order to understand some important features of Fig. 6, we turn to the action-angle variable representation (10), i.e.

$$H = \frac{\pi^2 J^2}{2} + \frac{2}{\pi^2\alpha} \sum_{\substack{n=-\infty \\ n\ odd}}^{\infty} \frac{1}{n^2} \sin(n\theta - t) \ .$$

If one now attempts a canonical transformation such that the new action and the new Hamiltonian are constants of motion to first order in α^{-1}, one finds that this perturbation theory breaks down near the *resonances*, where $\pi^2 J n = 1$, i.e., $u = \alpha/\pi n$, for any positive n. For large α, the resonances to lowest n (i.e., to highest energy), are widely separated, and in the neighborhood of such a resonance, the system is well approximated by a single resonance Hamiltonian

$$H_n = \frac{\pi^2 J^2}{2} + \frac{2}{\pi^2\alpha} \frac{\sin(n\theta - t)}{n^2} \ . \tag{16}$$

This Hamiltonian is integrable and becomes identical to the Hamiltonian for a pendulum under a canonical transformation that equals $\theta - t$ with the pendulum angle variable. For $\alpha = 165$, Fig. 6 shows clearly these pendulum–like trajectories. In [8], it was shown that the breakdown of the irrational tori between two resonance regions and the onset of large–scale chaos can be approximately determined from a two–resonance Hamiltonian that includes the two resonances adjacent to the considered torus. This chaotic region can be seen in the lower part of all three Figs. 6. The stable periodic orbits that can be seen for the larger two values of α represent trajectories that hit the walls always at the moment of farthest extension, as illustrated in Fig. 7, and they are at the center of resonance zones and correspond (in the single resonance approximation) to a pendulum at stable rest. The velocity of such a trajectory is given by

$$u_n^s = \frac{\alpha + 2}{(2n-1)\pi} \ . \tag{17}$$

The stability of these trajectories is found from linear stability analysis. The eigenvalues of the stability matrix are

$$\lambda_n = 1 - \frac{\pi}{u_n^s} \pm \sqrt{\frac{\pi}{u_n^s}(\frac{\pi}{u_n^s} - 2)} \ . \tag{18}$$

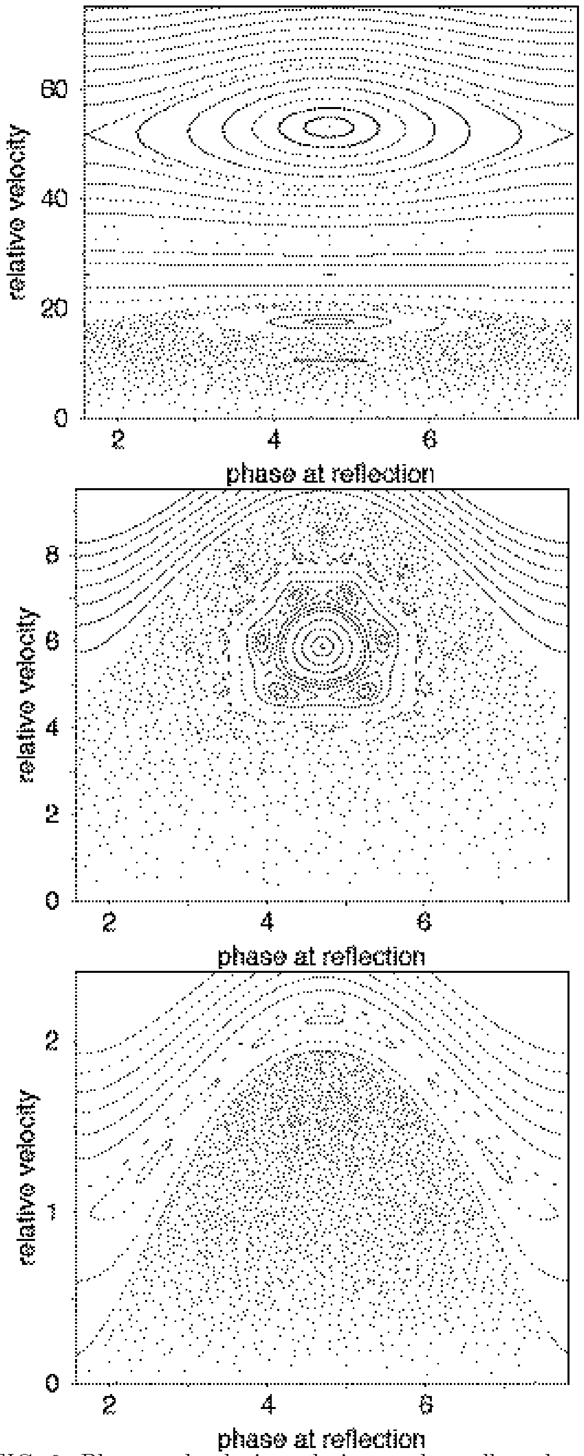

FIG. 6. Phase and velocity relative to the wall at the moment of reflection for α = 165, 16.5, and 1.65, for several different trajectories. To each trajectory, several 100 points are plotted.

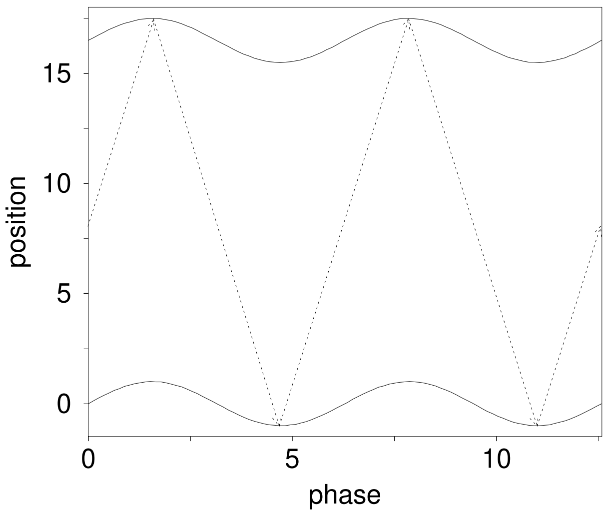

FIG. 7. The periodic orbit of lowest period.

For $u_n^s > \pi/2$ the eigenvalues are complex conjugate with $|\lambda| = 1$, and the trajectory is neutrally stable. For $u_n^s < \pi/2$, one eigenvalue is in modulus larger than one, and the trajectory is unstable. To each of these stable periodic orbits there exists an unstable counterpart that hits the walls always at phase $\pi/2$ and that has the velocity $u_n^u = (\alpha-2)/(2n-1)\pi$. These trajectories correspond (in the single resonance approximation) to a pendulum at its unstable fixed point. For nonintegrable systems, unstable periodic orbits are always part of chaotic regions. It is, however, remarkable, that the boundary of the large chaotic regions is close to such an unstable fixed point, and that its shape is close to the shape of a pendulum separatrix $u \simeq C_1 + C_2\sqrt{1-\sin\phi}$. This means that the separatrix belonging to the highest–energy resonance within the chaotic region determines the approximate boundary of the chaotic region.

For very large velocities $u \gg \alpha$, the phase and velocity relative to the wall change only by a small fraction between subsequent reflections, and solving a differential equation to leading order in $1/u$, one finds on approximate equation for the tori

$$u \simeq \sqrt{C - \alpha \sin\phi}\,.$$

(More generally, for a container oscillating according to an equation $x_{\rm wall} = f(\phi)$, one finds $u \simeq \sqrt{C - \alpha f''(\phi)}$.) This approximation can also be found from the Hamiltonian (10). A more detailed calculation including the first resonance gives

$$u \simeq \sqrt{\left(\frac{\alpha}{\phi}\right)^2 \left(1 + C' \pm \sqrt{C' - \frac{4}{\alpha}\sin\phi}\right) - \alpha\sin\phi} \quad (19)$$

The shape of stable irrational tori for smaller values of the velocity is obtained in [10] through approximation by periodic trajectories.

5. THE PARTIALLY INELASTIC PARTICLE

The dynamics of the partially elastic particle ($0 < \eta < 1$) show a very intricate structure. Depending on the parameters and the initial state, the trajectory of a particle can be on a low–periodicity periodic orbit, a strange attractor, or an orbit that looses periodically all its energy due to "chattering", i.e. an infinite number of reflections at the same wall during a finite time interval. In the following subsections we discuss all these phenomena and the interplay between them as the parameter values are varied.

5.1. Chattering

When the particle hits the wall with sufficiently small relative velocity, it is reflected infinitely often from that wall during a finite time interval and looses all its energy, as described in [7] for the vertically shaken particle. It subsequently sticks to the wall until the phase is $\phi = 0$, and then leaves the wall with relative velocity $u = 0$. In order to understand this phenomenon, let us consider first a particle colliding with a wall that is accelerated at a constant rate a. This situation is equivalent to a ball bouncing in a gravitational field, where it experiences a constant acceleration toward the ground. If the initial relative velocity of the particle is u_0, the relative velocity becomes zero after the time

$$T = 2\eta u_0/a + 2\eta^2 u_0/a + ... = 2u_0\eta/a(1-\eta)$$

after the first collision. In our system, the wall acceleration is of the order $A\omega^2$, and chattering can occur if the time T is no larger than of the order of the oscillation period ω^{-1}, leading to the condition $u_0 \lesssim A\omega(1-\eta)/\eta$ for chattering. For η close to 1, u_0 must be very small, which is only possible if the particle hits the wall at a phase ϕ_0 within a distance $\Delta\phi_0 \propto \sqrt{1-\eta}$ of π, or, equivalently, if the particle's trajectory hits the (absolute) position $x = 0$ (or $x = L$) within a time interval of the order $\Delta t \sim u_0\Delta\phi_0 \propto (1-\eta)^{3/2}$. The phase space volume $u_0\Delta t$ for which chattering occurs shrinks consequently as $(1-\eta)^{5/2}$, when η approaches 1.

In [7], it is argued that chattering is the generic fate of a particle bouncing on a vibrating platform, with the number of reflections between two chattering events diverging as η approaches 1. In our system, however, a particle that leaves the wall at phase $\phi = 0$ and with relative velocity $u = 0$, returns to the chattering region only for certain combinations of α and η, and is otherwise trapped on a periodic or chaotic orbit. Even in those cases where a chattered particle is chattered again, there may exist other trajectories that never enter the chattering region.

5.2. The almost elastic case

Due to dissipation, a given phase space volume shrinks with time. In particular, regions with large initial velocity are depleted, since the energy of a particle decreases exponentially fast until it reaches the regime where the time between impacts is of order unity, i.e. where its velocity is of order α. The change of u with the impact number n is approximately given by

$$\mathrm{d}u/\mathrm{d}n = -u(1-\eta)\,.$$

Using the relation $\mathrm{d}\phi \simeq (\alpha/u)\mathrm{d}n$, we find

$$u \simeq \frac{\alpha}{(1-\eta)(C+\phi)} \tag{20}$$

for the decrease of u with ϕ, with a constant C that is determined by the initial conditions. A small initial velocity interval consequently increases rapidly with increasing ϕ, leading to a strong shear of an initial domain of phase space, and interweaving different domains of attraction, as we shall see below. In fact, every domain of attraction contains points with arbitrarily large velocity.

Another consequence of the shrinking phase space volume is that all stable periodic orbits of a Hamiltonian system become attractive when small dissipation is added [11]. This is because the eigenvalues of the stability matrix remain complex conjugate for sufficiently small $(1-\eta)$, while their product is $\lambda_1\lambda_2 = \eta^2$, leading to $|\lambda_i| = \eta < 1$. Thus, for η infinitesimally smaller than 1, there is a plethora of attracting periodic orbits with competing domains of attraction. When η decreases further, most of these periodic orbits merge with unstable orbits and disappear, leaving only few attractive fixed points. The fixed points in the center of the resonances survive over a fairly large range of η values, as shown by the subsequent calculation. Writing

$$\rho = (2n-1)\pi\frac{1+\eta}{1-\eta}\,, \tag{21}$$

the fixed point in the center of the nth resonance changes with decreasing η according to

$$\sin\phi = \frac{2\alpha - \rho\sqrt{4+\rho^2-\alpha^2}}{4+\rho^2} \quad \text{and} \quad u = \frac{2\eta}{1-\eta}\cos\phi\,. \tag{22}$$

This fixed point can vanish by merging either with an unstable fixed point, or it can become unstable. The merging of stable and unstable fixed points occurs when the square root in (22) becomes imaginary, leading to the condition

$$\eta > \frac{\sqrt{\alpha^2-4}-(2n-1)\pi}{\sqrt{\alpha^2-4}+(2n-1)\pi} \tag{23}$$

for the existence of the fixed point.

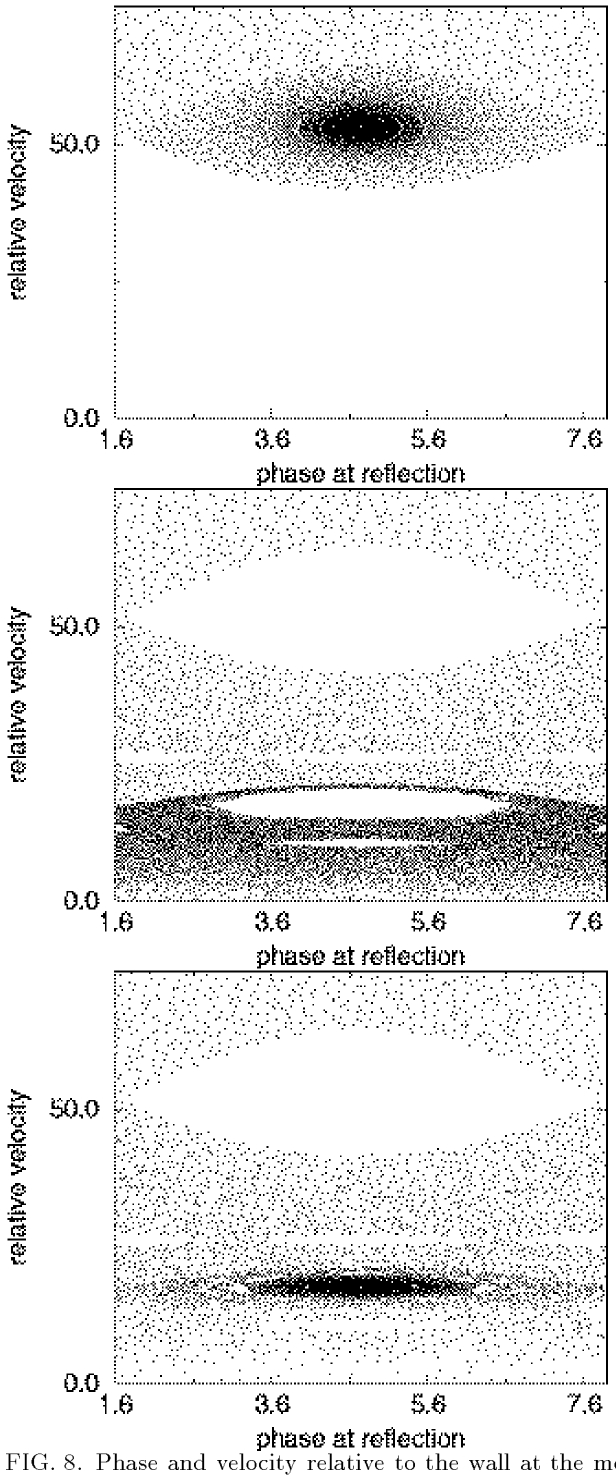

FIG. 8. Phase and velocity relative to the wall at the moment of reflection for $\alpha = 165$ and $\eta = 0.9999$, for three different trajectories. To each trajectory, 50000 points are plotted.

On the other hand, a stability analysis gives a stable fixed point for

$$-\frac{1+\eta}{1-\eta}\frac{2}{(2n-1)\pi} < \tan\phi < \frac{1-\eta}{1+\eta}\frac{2}{(2n-1)\pi}\,. \tag{24}$$

The violation of the left–hand side of condition (24) corresponds to a period doubling bifurcation (one eigenvalue becomes -1), the violation of the right–hand side corresponds to a saddle–node bifurcation (one eigenvalue becomes $+1$).

The chaotic regions surrounding the unstable fixed points for $\eta = 1$ also continue to influence the dynamics for $\eta < 1$. Typically [11], chaotic regions become transient when a small dissipation is added, and their main effect is the mixing of basins of attraction. In figure 8 we illustrate this for $\eta = 0.9999$, where we show three different orbits of particles starting at high initial velocities in the case $\alpha = 165$. One clearly sees the intertwining of different domains of attraction above the first resonance, making the fate of each particle appear random. After a long transient time, the first trajectory becomes trapped in the first resonance, the third trajectory in the second resonance, and the second trajectory is not yet trapped after 50000 reflections. It might either become attracted later by a higher–period orbit, or it might be chattered regularly. In the latter case, chatter should occur at intervals of the order of $(1-\eta)^{-5/2} \simeq 3 \times 10^{12}$ reflections (see previous subsection). A region that is chaotic for $\eta = 1$ is not immediately transformed into a strange attractor when η is decreased [11]. However, strange attractors occur for smaller values of η, as we shall see below.

5.3. Large dissipation

As we have seen in Section 3, every trajectory is periodic for $\eta = 0$ and may or may not go through the chattering region $\phi \in [\pi, 2\pi[\bmod 2\pi$. Both types of orbits can coexist for small η if the trajectory that starts in the chattering region is not trapped by the other periodic orbit. Since the basins of attraction of the chattering orbit and the normal periodic orbit are strongly interwoven, a small change in η can induce or remove such a trapping. When η is increased, normal periodic orbits typically go through a period–doubling scenario and then become a strange attractor. This attractor may be a global attractor, or it may coexist with other attractors, e.g., periodic orbits. Due to the large dissipation, the attractors are rather flat and seem almost one–dimensional in Poincaré like plots, as also known from other systems with large dissipation, like the Lorenz attractor [12]. Fig. 9 shows a strange attractor for $\alpha = 10$ and $\eta = 0.142$. The lower arches of the attractor correspond to the second, third, and fourth reflection at the same wall and are not present for smaller η. When η increases further, the number of arches diverges, and the attractor is replaced by a chattering orbit.

There are other mechanisms by which strange attractors may vanish with increasing η. As the attractor increases with η, its edge points may approach an unstable periodic orbit that ultimately diverts the trajectory from the attractor and leads it either into the chattering region, or to a stable periodic orbit that formerly coexisted with the attractor. Alternatively, as in the Feigenbaum scenario, an increase in η can induce a transition from a strange attractor to an intermittent periodic regime of some odd periodicity (e.g. 3), that undergoes in turn a period–doubling scenario. Even in cases where the attractor is destroyed due to chattering for some value of η, such intermittent periodic regimes and subsequent period–doubling cascades can still be observed when η is further increased.

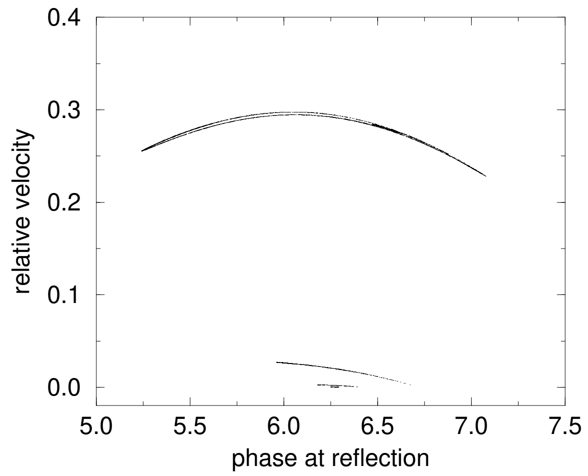

FIG. 9. The strange attractor for $\alpha = 10$ and $\eta = 0.142$.

Figure 10 shows the various attractors for $\alpha = 2$ as η is increased from 0 to 1. Increasing η from zero, we see a stable fixed point emerging from the chattering domain which dominates the dynamics at $\eta = 0$. This fixed point undergoes a complete period doubling scenario as η increases further. At the end of the period doubling scenario we have a chaotic attractor which continues to grow until it disappears when it overlaps with the chattering domain. The latter part of the period doubling scenario exists simultaneously with the stable three–cycle that is also shown in the figure. This three–cycle moves to the left as η increases, and it survives to $\eta = 1$. Close to $\eta = 1$, more periodic orbits exist that are not shown in the figure. Moreover, there are other small attractors which appear for intermediate values of η (some of the "dust" in the figure).

We have chosen $\alpha = 2$ for Fig. 10, as here the period doubling is clearly visible. For other values of α, more complicated scenarios can occur, as already indicated in the text above. There may be several period doubling cascades, which can occur for increasing as well as decreasing values of η. Period–doubling cascades for increasing η are usually initiated by an eigenvalue of the stability matrix of a periodic orbit becoming equal to -1, while cascades for decreasing η occur when a periodic trajectory starts to experience several reflections at the same wall. Moreover, there can be intervals of η for which all trajectories experience chattering, i.e., where the only attractor is the periodic orbit with chattering. Period–doubling cascades are also observed when α is varied for fixed η.

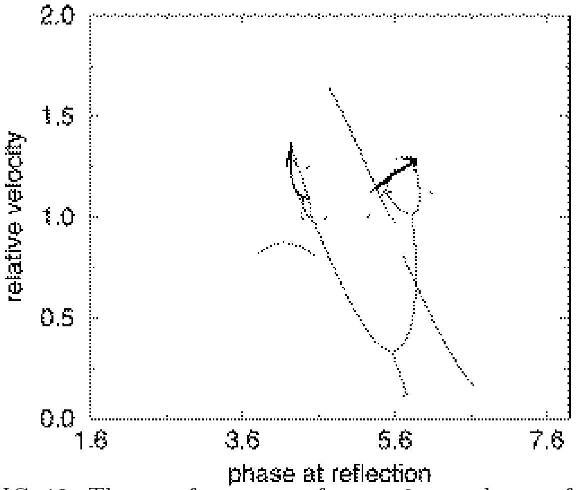

FIG. 10. The set of attractors for $\alpha = 2$ as η changes from 0 to 1.

5.4. Ghost attractors and domains of attraction

Since the size of strange attractors increases with increasing η until they become absorbed by the chattering orbit, strange attractors become rare for higher values of η. Nevertheless, the "ghosts" of these attractors still continue to influence the dynamics by trapping trajectories for a transient time, which can last several hundred or thousand reflections. Consequently, the domains of attraction for normal periodic and chattering orbits become strongly interwoven, as shown in Fig. 11 for $\alpha = 10$ and $\eta = 0.61575$. There is a fixed point sitting in the center of the curl, and there is one chattering orbit. The large black and white areas around the curl are the domain of attraction of the fixed point, and the two colours distinguish between trajectories that need an even or odd number of reflections before reaching some small region around the fixed point. The area with the irregularly distributed black dots is the region where the domains of attraction of the fixed point and the chattering orbit are interwoven, the black dots being points that utimately become attracted to the fixed point. For two nearby starting points in this region, the trajectories follow a "ghost attractor", by which they are trapped for quite some time. The release of the trajectories to either the attracting fixed point or the chattering domain is seemingly random due to the influence of the attractor, as can be seen from the bottom figure. The white region at the bottom of the top figure belongs entirely to the basin of attraction of the chattering orbit.

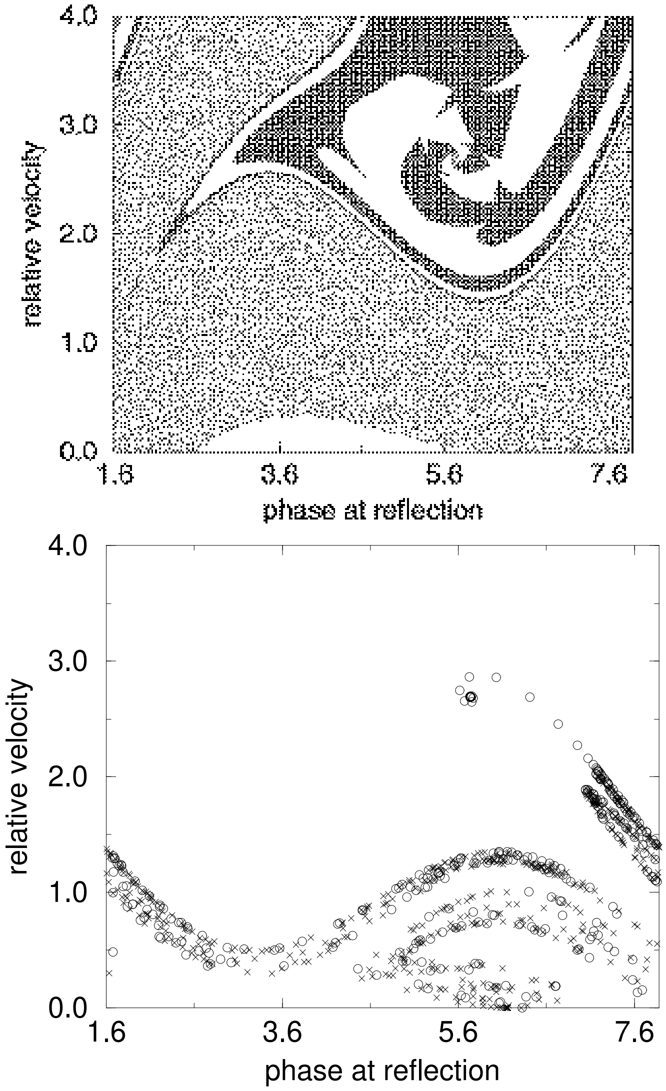

FIG. 11. The two domains of attraction for $\alpha = 10$ and $\eta = 0.61578$. The attracting fixed point is at $\phi \approx 5.7$ and $u \approx 2.7$. Chattering occurs immediately for orbits entering the white domain at the bottom of the upper figure, and trajectories starting in the large black and white areas around the fixed point become absorbed in a small neighborhood around the fixed point after an even resp. odd number of steps. In the region with the irregularly placed black dots, trajectories are strongly mixed, and it cannot be predicted whether they will be chattered or absorbed at the fixed point. The lower figure illustrates how how two nearby trajectories follow a "ghost attractor", before they eventually either chatter or get attracted to the fixed point.

5.5. The influence of friction

For the case of a completely inelastic particle, we have studied in Section 3 the influence of friction between the particle and the container bottom. Particles that are so slow that they cannot reach the other wall become trapped in the region between the walls, where they perform a low–amplitude periodic oscillation. For sufficiently large container sizes, this is the fate of all particle trajectories. A similar behaviour can be expected when the coefficient of restitution does not vanish. All orbits that extend to a region of sufficiently low velocity will become trapped in the region between the walls. This will in particular affect long orbits like chattering orbits and strange attractors. For the completely elastic case, even a small amount of friction destroys the hamiltonian nature of the system, and we expect that the system behaves similar to the situation where the coefficient of restitution is slightly smaller than 1. Thus, we expect all stable periodic orbits to become attractive, and all chaotic regions to become transient for an infinitesimally small amount of friction.

6. CONCLUSION AND OUTLOOK

In this paper, we have shown that a particle in a horizontally shaken box shows a much richer behaviour than a particle on a vibrating platform. While chattering, i.e., the loss of all kinetic energy during a finite time, may occur for any value of the coefficient of restitution smaller than one, other scenarios like period–doubling and strange attractors are observed as well. We have also discussed the interplay and transitions between these scenarios, and the influence of friction between the particle and the container bottom. We know only of one other system where the interplay between chattering, chaos, and periodic orbits has been studied before, namely the forced oscillator impacting on a wall [13].

The chattering phenomenon discussed in this paper is a good approximation to reality only when the collision time between the particle and the wall is much shorter than the oscillation period. If this condition is not satisfied, the deformation of the particle during the collision has to be included in the model, thus adding another degree of freedom.

When $N > 1$ particles are placed in the container, new phenomena will arise. Three or more particles with a sufficiently small coefficient of restitution $\eta < 1 - 1/N$ are known to undergo an *inelastic* collapse, where they loose all their relative kinetic energy due to infinitely many collisions during a finite time [14,15], a phenomenon similar to chatter. But even for parameter values that do not allow for an inelastic collapse, clustering phenomena occur. In [16], a system with one elastic and one thermally moving wall is studied for approximately ten particles. The authors find that most of the particles form a cluster almost at rest, while a few remaining particles travel between the boundaries at a much higher speed. We have seen a slightly different phenomenon in the periodically shaken box, namely the formation of two clusters travelling between the boundaries and the center of the system, similar to Newton's cradle.

ACKNOWLEDGMENTS

This work was supported by EPSRC Grant No. GR/K79307.

[1] Straßburger, G., Betat, A., Scherer, M.A., Rehberg, I.: in *Traffic and Granular Flow*, Wolf, D.E., Schreckenbach, M., and Bachem, A. (eds.) (World Scientific, 1996)
[2] Ristow, G.H., Straßburger, G., and Rehberg, I.: Phys. Rev. Lett. **79**, 833 (1997)
[3] Melo, F., Umbanhowar, P., Swinney. H.L: Phys. Rev. Lett. **72**, 172 (1994); *ibid* **75**, 3838 (1995)
[4] Umbanhowar, P., Melo, F., Swinney, H.L.: Nature **382**, 793 (1996)
[5] Clement, E. et al.: Phys. Rev. E **53**, 2972 (1996)
[6] Mehta, A., Luck, J.M.: Phys. Rev. Lett. **65**, 393 (1990)
[7] Luck, J.M., Mehta, A.: Phys. Rev. E **48**, 3988 (1993)
[8] Lin, W.A., Reichl, L.E.: Physica D **19**, 145 (1986)
[9] Reichl, L.E.: *The Transition to Chaos in Conservative Classical Systems: Quantum Manifestations* (Springer–Verlag, New York, 1992)
[10] Fuka, M.Z.: Phys. Rev. E **51**, 1935 (1995)
[11] Lieberman, M.A., Tsang, K.Y.: Phys. Rev. Lett. **55**, 908 (1985)
[12] For an beautiful introduction to the Lorenz and other strange attractors see e.g. the chapters 9 to 12 of Strogatz, S.H.: *Nonlinear Dynamics and Chaos* (Addison–Wesley, Reading, MA, 1994)
[13] Budd, C., Dux, F., and Cliffe, A: Journal of Sound and Vibration **184**, 475 (1995)
[14] McNamara, S., Young, W.R.: Phys. Fluids A **4**, 496 (1992)
[15] Zhou, T., Kadanoff, J.P.: Phys. Rev. E **54**, 623 (1996)
[16] Du, Y., Li, H., Kadanoff, L.P.: Phys. Rev. Lett. **74**, 1268 (1995)